Chemical Physics 391 (2011) 69–77

Contents lists available at ScienceDirect

Chemical Physics

journal homepage: www.elsevier.com/locate/chemphys

# An efficient method for quantum transport simulations in the time domain

Y. Wang [a], C.-Y. Yam [a,b], Th. Frauenheim [a], G.H. Chen [b], T.A. Niehaus [c,*]

[a] Bremen Center for Computational Materials Science, University of Bremen, Germany
[b] Department of Chemistry, The University of Hong Kong, Hong Kong, China
[c] Department of Theoretical Physics, University of Regensburg, 93040 Regensburg, Germany

ARTICLE INFO

*Article history:*
Available online 12 April 2011

*Keywords:*
Time dependent density functional theory
Quantum transport
Molecular electronics
DFTB

ABSTRACT

An approximate method based on adiabatic time dependent density functional theory (TDDFT) is presented, that allows for the description of the electron dynamics in nanoscale junctions under arbitrary time dependent external potentials. The density matrix of the device region is propagated according to the Liouville–von Neumann equation. The semi-infinite leads give rise to dissipative terms in the equation of motion which are calculated from first principles in the wide band limit. In contrast to earlier *ab initio* implementations of this formalism, the Hamiltonian is here approximated in the spirit of the density functional based tight-binding (DFTB) method. Results are presented for two prototypical molecular devices and compared to full TDDFT calculations. The temporal profile of the current traces is qualitatively well captured by the DFTB scheme. Steady state currents show considerable variations, both in comparison of approximate and full TDDFT, but also among TDDFT calculations with different basis sets.


## 1. Introduction

Molecular electronics – the use of single molecules as functional entities in electronic devices – is often heralded as a replacement for the conventional CMOS technology which faces physical limits in further miniaturization. Even if the industrial application of this technology seems to be out of reach in the moment, research on the electronic transport through individual molecules has already revealed a variety of interesting quantum phenomena. To these belong strong electron correlation giving rise to Coulomb blockade and Kondo physics, electron–phonon interactions responsible for device heating and measurable in inelastic tunneling spectra, as well as electron–photon interactions for molecular photo-switches [1]. While a qualitative understanding of these complex processes has been obtained in many cases, quantitative agreement between first-principles theory and experiment is still unsatisfactory for the seemingly simple case of ballistic steady state transport [2].

The majority of such studies for realistic devices are based on the nonequilibrium Green's function (NEGF) technique [3], which reduces to the traditional Landauer transmission formalism [4,5] for coherent transport. The device Green's function is then constructed from the Kohn–Sham (KS) single-particle Hamiltonian of ground state density functional theory (DFT) including the effects of the leads through suitable self-energies. For finite bias, more sophisticated approaches determine the actual potential profile on the molecule by solving the Poisson equation in order to achieve a self-consistent treatment of Hamiltonian and Green's function [1].

In recent years, also time-dependent density functional theory (TDDFT) has become popular in the context of molecular electronics [6–13]. The reason for this is twofold. First, TDDFT goes beyond the *ad hoc* application of the DFT Hamiltonian for non-equilibrium systems and provides a more rigorous theoretical foundation [14]. In fact, calculations at this level provide corrections to the conventional DFT-NEGF results for steady state currents, provided nonlocal exchange–correlation functionals are employed [15–18]. Second, TDDFT allows for the description of dynamical processes like the switching behavior of molecular devices and alternating currents. The formalism may also be easily extended to cover the interaction with light, which paves the way to study photo-assisted and photo-suppressed transport, the fluorescence of contacted molecules or atomistic opto-electronic devices like photoswitches.

So far, several implementations of TDDFT for open systems have been suggested, which may be classified according to the way the transport boundary conditions are treated. The simplest approach is to approximate the mesoscopically large leads by atomic clusters of finite size [6,9,11,13]. The Kohn–Sham orbitals are then time-propagated under the influence of a potential difference between left and right leads and changes of molecular charges in the contacts allow one to quantify the current. This approach has the advantage that TDDFT algorithms for isolated systems can be applied to the transport scenario without large changes. On the downside, a steady-state current is only transiently reached due to charge accumulation. Also, unphysical oscillations of the current

* Corresponding author.
*E-mail address:* thomas.niehaus@physik.uni-regensburg.de (T.A. Niehaus).

0301-0104/$ - see front matter © 2011 Published by Elsevier B.V.
doi:10.1016/j.chemphys.2011.04.006

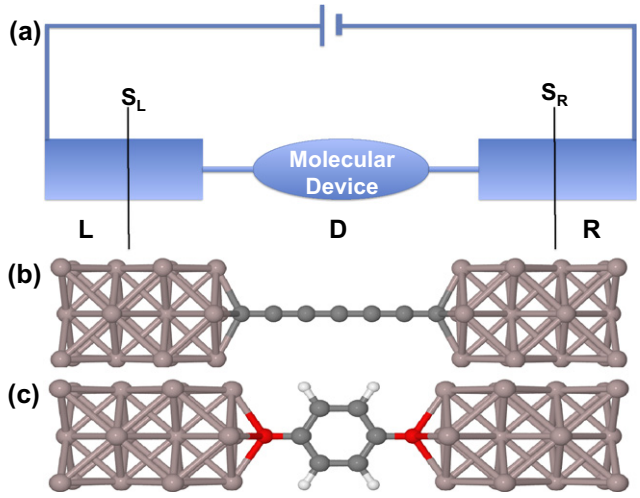


**Fig. 1.** (a) Schematic device setup with D denoting the central device region. The left (L) and right (R) leads are assumed to be semi-infinite and in thermal equilibrium. (b) Seven-membered carbon chain between Al nanowires in (001) direction. Frontier carbon atoms in hollow position of the Al surface at 1.0 Å distance. Bond lengths (Å): C–C = 1.32, Al–Al = 2.86. (c) 1, 4-benezenediol molecule inbetween Al nanowires.

never fully die out, because of the discrete level spectrum of the contacts.

Another path was pursued by Burke and co-workers [8,19]. Here a ring-topology of the electronic circuit is used to avoid the conceptual difficulty of having two different chemical potentials as in the Landauer picture. A constant electric field on the ring is used to generate a current and coupling to a heat bath within a master equation approach allows for the establishment of a steady-state.

A third approach is given by a separation of the conductor into a finite device region and two semi-infinite leads, very similar to the treatment within the standard DFT-NEGF approach (see Fig. 1(a)). The time-dependent Kohn–Sham equations need to be solved for the central region only and the effect of the leads is exactly accounted for by properly defined self-energies. Several model studies along these lines are documented in the literature [10,20–22]. Finally, a closely related path is followed by Chen and co-workers [12,23,24]. Instead of propagating Kohn–Sham states, the equations of motion are written in terms of the reduced density matrix for the device region. This fact allows one to obtain the initial conditions from a straightforward application of equilibrium Green's function theory.

For all of the methods mentioned above, simulations on realistic molecular devices which take the atomistic structure of both molecule and leads into account are numerically demanding. This is because the electron motion has to be fully resolved, leading to time steps in the sub-fs range. Although only the central part of the device is out of equilibrium, this region has to include several layers of the lead material in addition to the functional molecule in question, which raises the dimension of the Hamiltonian. Only in this way a smooth transition of potentials at the device-lead interface is guaranteed. Moreover, comprehensive studies require numerous simulations involving the variation of different parameters, like different molecular binding configurations, temporal bias profiles or light frequency and amplitude in case of photo-induced processes. Hence, a computationally efficient, but still predictive method based on TDDFT seems to be desirable.

In this contribution we present efforts in this direction and discuss an implementation of the density functional based tight-binding method (DFTB) [25–27] for open systems. The ground state DFTB approach is characterized by several additional approximations beyond a particular exchange–correlation functional and has already been generalized to the time domain (TD-DFTB, [28–30]) in the spirit of TDDFT. Here we follow the mentioned density matrix approach of Chen and co-workers to arrive at a fast simulation method for open systems driven by time dependent bias potentials. In Section 2 the basic equations of motion are reviewed, while Section 3 discusses the approximations underlying the DFTB scheme and the necessary adaptions in the present context. Several case studies are presented in Section 4 followed by a brief summary and outlook in Section 5.

## 2. Equation of motion for the reduced density matrix

### 2.1. General formulas

We consider a system as depicted in Fig. 1(a) and aim at evaluating the current through the central device region (D) which is driven by a time-dependent bias potential $V(t)$. The left (L) and right (R) lead are thought to extend from the device region to infinity and feature a continuous density of states to ensure proper dissipation. In second quantization, the electronic Hamiltonian of the whole system can be written as

$$\mathcal{H}_{\mathrm{tot}} = \sum_{mn} H_{mn} d_m^\dagger d_n + \sum_{\alpha,k} \varepsilon_{\alpha,k} c_{\alpha,k}^\dagger c_{\alpha,k} + \sum_{\alpha,k;m} \left( T_{\alpha,k;m} c_{\alpha,k}^\dagger d_m + \mathrm{h.c.} \right). \tag{1}$$

Here, the first term describes the device region, where $d_m^\dagger(d_m)$ is the creation (annihilation) operator for an electron in the atomic orbital $m$, and $H_{mn}$ stands for the corresponding Hamiltonian in this basis. The second term describes the contacts ($\alpha \in \{\mathrm{L}, \mathrm{R}\}$), where $c_{\alpha,k}^\dagger(c_{\alpha,k})$ is the creation (annihilation) operator for an electron in the single-particle state $k$ in the $\alpha$th contact, while $\varepsilon_{\alpha,k}$ is the corresponding level energy. The third term describes the coupling between device region and contacts and features the hopping matrix $\boldsymbol{T}$ (matrices will be denoted by bold face letters). Although the Hamiltonian in Eq. (1) is formally valid only for non-interacting particles, the yet to be specified parameters may effectively account for electron–electron interactions, for example in a DFT context. Moreover, a self-consistent determination of the device Hamiltonian and hopping matrix will result in a time dependence of these quantities for varying external bias.

Next, we define the lesser Green's function [31] of the device region as

$$G_{mn}^<(t,t') = i\left\langle d_n^\dagger(t') d_m(t) \right\rangle \tag{2}$$

and apply the equation of motion for Heisenberg operators to arrive at

$$i\frac{\partial}{\partial t}\boldsymbol{G}^<(t,t') = [\boldsymbol{H}, \boldsymbol{G}^<(t,t')] + \sum_\alpha \boldsymbol{Q}_\alpha(t,t'), \tag{3}$$

where $\boldsymbol{Q}_\alpha(t,t')$ is given in terms of the coupling matrix and the lead-device lesser Green's function

$$G_{\alpha,k;n}^<(t,t') = i\left\langle d_n^\dagger(t') c_{\alpha,k}(t) \right\rangle, \tag{4}$$

as follows

$$Q_{\alpha,mn}(t,t') = \sum_k [T_{m;\alpha,k}(t) G_{\alpha,k;n}^<(t,t') - G_{m;\alpha,k}^<(t,t') T_{\alpha,k;n}(t')]. \tag{5}$$

Following the standard NEGF technique [31], the term $\boldsymbol{Q}_\alpha(t)$ can be further rewritten in a form that incorporates only matrices with the dimension of the device region:

$$\boldsymbol{Q}_\alpha(t,t') = +\int_{-\infty}^{+\infty} d\tau\left[\boldsymbol{\Sigma}_\alpha^r(t,\tau)\boldsymbol{G}^<(\tau,t') + \boldsymbol{\Sigma}_\alpha^<(t,\tau)\boldsymbol{G}^a(\tau,t')\right] - \int_{-\infty}^{+\infty} d\tau\left[\boldsymbol{G}^<(t,\tau)\boldsymbol{\Sigma}_\alpha^a(\tau,t') + \boldsymbol{G}^r(t,\tau)\boldsymbol{\Sigma}_\alpha^<(\tau,t')\right]. \quad (6)$$

Here, $\boldsymbol{G}^{r(a)}$ are the retarded (advanced) Green's functions of the device region, which satisfy the Dyson equation

$$\left(i\frac{\partial}{\partial t} - \boldsymbol{H}(t)\right)\boldsymbol{G}^{r(a)}(t,t') - \sum_\alpha \int_{-\infty}^{+\infty} d\tau\boldsymbol{\Sigma}_\alpha^{r(a)}(t,\tau)\boldsymbol{G}^{r(a)}(\tau,t') = \delta(t-t'), \quad (7)$$

while $\boldsymbol{\Sigma}_\alpha^{r,a,<}$ are the retarded (advanced, lesser) self-energies due to the coupling to the $\alpha$th contact. They are given as

$$\boldsymbol{\Sigma}_\alpha^{r,a,<}(t,\tau) = \boldsymbol{T}_\alpha^\dagger(t)\boldsymbol{g}_\alpha^{r,a,<}(t,\tau)\boldsymbol{T}_\alpha(\tau), \quad (8)$$

with $\boldsymbol{g}_\alpha^{r,a,<}$ denoting the Green's functions of the $\alpha$th contact.

Eqs. (3) and (6)–(8) form a closed set of equations to describe the dynamical properties of non-equilibrium systems and will be the theoretical basis of our method. Instead of working with the full lesser Green's function, a significant simplification is achieved by turning to the reduced density matrix for the device region ($\boldsymbol{\sigma}(t)$) as the key quantity, which is dependent on a single time argument only. The quantity $\boldsymbol{\sigma}(t)$ is directly related to the lesser Green's function $\boldsymbol{G}^<(t,t')$

$$\boldsymbol{\sigma}(t) = -i\boldsymbol{G}^<(t,t). \quad (9)$$

Thus, the equation of motion for $\boldsymbol{\sigma}(t)$ can be obtained from Eq. (3) as

$$i\frac{\partial}{\partial t}\boldsymbol{\sigma}(t) = [\boldsymbol{H}(t),\boldsymbol{\sigma}(t)] - i\sum_\alpha \boldsymbol{Q}_\alpha(t). \quad (10)$$

For vanishing coupling (i.e. $\boldsymbol{T} = 0$), $\boldsymbol{Q}$ vanishes and Eq. (10) reduces to the conventional quantum Liouville equation for closed systems. The quantity $\boldsymbol{Q}_\alpha$ describes dissipation effects due to the presence of the semi-infinite contacts and gives rise to finite lifetimes of states located in the central region. It is also noted that the trace of the matrix $\boldsymbol{Q}_\alpha$ gives the particle current through the interface $S_\alpha$ (see Fig. 1(a)) in contact $\alpha$ [12]

$$I_\alpha(t) = -\mathrm{Tr}[\boldsymbol{Q}_\alpha(t)]. \quad (11)$$

### 2.2. Wide-band approximation for the dissipation term $\boldsymbol{Q}_\alpha$

Direct application of Eq. (6) to evaluate the dissipation term $\boldsymbol{Q}_\alpha$ turns out to be computationally demanding. This is due to the necessity to store and integrate over two-time quantities like the self-energies. A common solution is to invoke the wide band approximation (WBA), where both the lead density of states and the device-lead coupling are assumed to be smooth and not strongly dependent on energy. This is a reasonable approximation for simple metals in the linear response regime but fails for larger applied bias and/or leads with a more complex density of states, like for example nanotubes. The WBA is however not without alternative in the present context. Recently, Zheng and co-workers presented a hierarchical equation of motion approach, which goes beyond the WBA at a tolerable increase in computational effort [24].

Within the WBA, the self-energies $\boldsymbol{\Sigma}_\alpha^{r/a}$ become local in time and can be written as [12]

$$\boldsymbol{\Sigma}_\alpha^{r,a}(t,t') = (\boldsymbol{\Gamma}_\alpha \mp i\boldsymbol{\Lambda}_\alpha)\delta(t-t'). \quad (12)$$

Here, the matrices $\boldsymbol{\Gamma}_\alpha$ and $\boldsymbol{\Lambda}_\alpha$ denote the hermitian and anti-hermitian part of $\boldsymbol{\Sigma}_\alpha^a(E)$, respectively,[1] and are evaluated at the common Fermi energy ($E_F$) of the unbiased system. Assuming that the non-interacting electrons in contact $\alpha$ are in local equilibrium characterized by a Fermi–Dirac distribution function $f^\alpha(\epsilon)$ with chemical potential $\mu_0$ and assuming further that the bias potential $V_\alpha(t)$ leads to a rigid shift of the lead energy levels, one obtains

$$\boldsymbol{\Sigma}_\alpha^<(t,t') = \frac{2i}{\pi}\boldsymbol{\Lambda}_\alpha \exp\left\{i\int_{t'}^t d\tau V_\alpha(\tau)\right\}\int_{-\infty}^{+\infty} d\epsilon f^\alpha(\epsilon)e^{-i\epsilon(t-t')}. \quad (13)$$

With the expressions (12) and (13) above, the dissipation term $\boldsymbol{Q}_\alpha(t)$ can be simplified to [12]

$$\boldsymbol{Q}_\alpha(t) = i[\boldsymbol{\Gamma}_\alpha,\boldsymbol{\sigma}(t)] + \{\boldsymbol{\Lambda}_\alpha,\boldsymbol{\sigma}(t)\} + \boldsymbol{K}_\alpha(t). \quad (14)$$

Here, the first term represents the renormalization of the device energy levels due to the $\alpha$th contact and involves a commutator; the second term involving an anti-commutator describes the level broadening, while the hermitian matrix $\boldsymbol{K}_\alpha(t)$

$$\boldsymbol{K}_\alpha(t) = -\frac{2i}{\pi}\boldsymbol{U}_\alpha(t)\int_{-\infty}^{\mu_0}\frac{d\epsilon e^{i\epsilon t}}{\epsilon\boldsymbol{I} - \boldsymbol{H}(0) - \boldsymbol{\Sigma}^r}\boldsymbol{\Lambda}_\alpha - \frac{2i}{\pi}\int_{-\infty}^{\mu_0}[\boldsymbol{I} - \boldsymbol{U}_\alpha(t)e^{i\epsilon t}]\frac{d\epsilon}{(\epsilon - V_\alpha(t))\boldsymbol{I} - \boldsymbol{H}(t) - \boldsymbol{\Sigma}^r}\boldsymbol{\Lambda}_\alpha + \mathrm{h.c.}, \quad (15)$$

incorporates the history of the applied bias via the propagator $\boldsymbol{U}_\alpha(t)$

$$\boldsymbol{U}_\alpha(t) = \exp\left\{-i\int_0^t[\boldsymbol{H}(\tau) + \boldsymbol{\Sigma}^r - \boldsymbol{I}V_\alpha(\tau)]d\tau\right\}. \quad (16)$$

The term $\boldsymbol{\Sigma}^r$ is a summation of the retarded self-energy functions for both contacts.

Eqs. (10) , (14)–(16) provide an approximate approach to calculate the transient non-equilibrium density matrix for open systems. Zheng et al. have combined the scheme described above with TDDFT to simulate the time-dependent transport in nanoscale systems [12,23]. Next, we will describe how the density matrix $\boldsymbol{\sigma}(t)$, Hamiltonian $\boldsymbol{H}(t)$, and dissipation term $\boldsymbol{Q}_\alpha(t)$ are constructed in the framework of the density-functional based tight-binding (DFTB) method, which aims to provide a more efficient but still accurate method for real material simulations.

## 3. Density functional based tight-binding method

### 3.1. DFTB for closed systems

As an approximate DFT method, DFTB was initially developed to study the ground state of finite or periodic systems. Details on the derivation and performance for these class of materials may be found in several reviews [32–34]. As in conventional tight-binding models, the total energy of DFTB consists of a band structure part $E_{\mathrm{BS}}$ and a repulsive energy part $E_{\mathrm{rep}}$,

$$E^{\mathrm{DFTB}} = E_{\mathrm{BS}} + E_{\mathrm{rep}}. \quad (17)$$

Since we will not consider structural changes during electron transport in the present work, only the band structure term is relevant for the further discussion. It takes the form

$$E_{\mathrm{BS}} = \sum_i^{\mathrm{occ}}\langle\Psi_i|H_0|\Psi_i\rangle + \frac{1}{2}\sum_{\alpha,\beta}\gamma_{\alpha\beta}\Delta q_\alpha\Delta q_\beta, \quad (18)$$

which is obtained through an expansion of the DFT total energy around a reference density $n^0(\boldsymbol{r})$ up to second order [27]. The latter is taken to be a superposition of the neutral densities of all atoms comprising the system in question ($n^0(\boldsymbol{r}) = \sum_\alpha n_\alpha^0(\boldsymbol{r})$). The first term in Eq. (18) involves a sum over expectation values of the DFT Hamiltonian evaluated at $n^0$:

$$H_0(\boldsymbol{r}) = -\frac{\nabla^2}{2} + V_{ext}(\boldsymbol{r}) + \int d\boldsymbol{r}'\frac{n_0(\boldsymbol{r}')}{|\boldsymbol{r} - \boldsymbol{r}'|} + V_{\mathrm{XC}}[n_0] \quad (19)$$

[1] Note that the definition of $\boldsymbol{\Gamma}_\alpha$ and $\boldsymbol{\Lambda}_\alpha$ is often interchanged in the literature. We keep with the notation of Ref. [12] to ease comparison.

with the kinetic energy operator, the external potential, the Hartree potential generated by $n_0$ and the DFT exchange–correlation potential.

The last quantity in Eq. (18) represents the second-order term in the mentioned density expansion and accounts for charge transfer effects. Here, $\Delta q_\alpha$ is defined as the difference of the Mulliken charges between charged and neutral atom $\alpha$, i.e. $\Delta q_\alpha = q_\alpha - q_\alpha^0$. The matrix $\gamma_{\alpha\beta}$ is a measure of the electron–electron interaction and decays like $1/|\boldsymbol{R}_\alpha - \boldsymbol{R}_\beta|$ for large distances between atoms at $\boldsymbol{R}_\alpha$ and $\boldsymbol{R}_\beta$. For the on-site case, the Hubbard-like parameter $U_\alpha = \gamma_{\alpha\alpha}$ is taken from full atomic DFT calculations and represents the chemical hardness of the respective element. An interpolation formula between these limiting cases can be analytically constructed [27] by invoking a monopole approximation for the density fluctuations $\delta n_\alpha$, which are assumed to take the form

$$\delta n_\alpha(\boldsymbol{r}) = \frac{\Delta q_\alpha \tau_\alpha^3}{8\pi} e^{-\tau_\alpha|\boldsymbol{r}-\boldsymbol{R}_\alpha|}, \quad \text{with} \quad \int d\boldsymbol{r}\delta n_\alpha(\boldsymbol{r}) = \Delta q_\alpha. \tag{20}$$

Here, the effective decay constant $\tau_\alpha = \frac{16}{5}U_\alpha$ is determined by the constraint $U_\alpha = \gamma_{\alpha\alpha}$.

In the practical implementation of DFTB, the Kohn–Sham orbitals $|\Psi_i\rangle$ are expanded in a set of localized atomic orbitals (AO) $\{|\phi_\mu\rangle\}$ that are again obtained from a full atomic DFT calculation

$$|\Psi_i\rangle = \sum_\mu c_{i\mu}|\phi_\mu\rangle. \tag{21}$$

Usually only occupied AO are used in the molecular expansion, but this is not a necessary requirement of the model. The atomic DFT calculations are converged with respect to the basis set size, so that each AO is constructed from a superposition of many Slater-type orbitals. Furthermore, an additional confinement potential in the atomic calculations leads to a suppression of the long-range tail of the AO, making them suitable expansion functions for the molecular case [26]. The minimal basis set of DFTB is expected to be more accurate than conventional contracted basis sets of the same size, e.g. Pople's STO-3G.

In a two-center approximation, matrix elements of the DFT Hamiltonian in Eq. (19) $\left(H^0_{\mu\nu}\right)$ are numerically computed and stored in Slater–Koster [35] tables as function of the inter-element distance. The Mulliken charges used to estimate the second-order term in the density expansion are given in terms of the molecular orbital coefficients ($c_{i\mu}$) and the overlap of two atomic orbitals ($S_{\mu\nu} = \langle\phi_\mu|\phi_\nu\rangle$):

$$q_\alpha = \mathrm{Tr}_\alpha[\boldsymbol{\sigma}S] = \frac{1}{2}\sum_i^{occ}\sum_{\mu\in\alpha}\sum_\nu\left(c^*_{i\mu}c_{i\nu}S_{\mu\nu} + c^*_{i\nu}c_{i\mu}S_{\nu\mu}\right). \tag{22}$$

The trace is performed over all atomic orbitals on site $\alpha$ and $\boldsymbol{\sigma}$ denotes the density matrix in the AO basis. Thus the total energy of DFTB will be a function of the expansion coefficients $\left\{c_{i\mu}, c^*_{j\nu}\right\}$ in the given basis set. The ground state energy can be obtained from the variational principle

$$\delta\left(E_{BS} - \sum_i \epsilon_i c^*_{i\mu}c_{i\nu}S_{\mu\nu}\right)\Big/\delta c^*_{j\mu} = 0, \tag{23}$$

where the $\epsilon_i$ are Lagrange multipliers.

The solution of Eq. (23) gives rise to the secular equation

$$\sum_\nu (H_{\mu\nu} - \epsilon_i S_{\mu\nu})c_{i\nu} = 0, \tag{24}$$

where the Hamiltonian matrix element $H_{\mu\nu}$ for atom pair ($\alpha$, $\beta$) reads

$$H_{\mu\nu} = H^0_{\mu\nu} + \frac{1}{2}S_{\mu\nu}\sum_\gamma(\gamma_{\alpha\gamma} + \gamma_{\beta\gamma})\Delta q_\gamma \quad \mu\in\alpha, \quad \nu\in\beta. \tag{25}$$

Eq. (24) can be viewed as an approximate version of the Kohn–Sham equation in DFT. The second term in (25) accounts for changes of the electron density with respect to the reference ($n^0$) and needs to be determined self-consistently via repeated evaluation of Eqs. (24), (22), and (25), very similar to self-consistent field approaches. The computational efficiency of the DFTB method grounds on two facts. First, the minimal but still accurate basis set is smaller then in conventional DFT approaches and second, the construction of the Hamiltonian requires little CPU time due the precomputation of all numerical integrals.

### 3.2. DFTB for open systems

For open systems, the concept of a total energy is not well-defined, and the variational principle and secular equation do not hold. Thus, the DFTB method needs to be generalized in oder to deal with a semi-infinite system out of equilibrium. Recalling the Eqs. (10) and (14)–(16) in Section 2 which describe the transient non-equilibrium dynamics in open systems, the key ingredients which determine the reduced density matrix $\boldsymbol{\sigma}(t)$ are the Hamiltonian $\boldsymbol{H}(t)$ and self-energy functions $\boldsymbol{\Sigma}_\alpha$. Here we present how to construct these matrices in the framework of DFTB.

#### 3.2.1. Device Hamiltonian

In the spirit of DFTB, the Hamiltonian should take the general form

$$H_{\mu\nu} = H^0_{\mu\nu}[n_0] + \delta V_{\mu\nu}[\{\Delta q_\alpha\}], \tag{26}$$

where the first term is the zero-order DFTB Hamiltonian, while the second term includes the Hartree potential $\delta V_H$ and exchange–correlation potential $\delta V_{XC}$ due to the difference density $\delta n = \sum_\alpha \delta n_\alpha$.

For closed systems, where the electrostatic potential can be assumed to tend to zero at infinity, the Hartree potential $\delta V_H(\boldsymbol{r})$ is given by

$$\delta V_H(\boldsymbol{r}) = \int d\boldsymbol{r}'\frac{\delta n(\boldsymbol{r}')}{|\boldsymbol{r}-\boldsymbol{r}'|}. \tag{27}$$

Using Eq. (20), this results in the $\gamma$-matrix dependent second-order term of the Hamiltonian in Eq. (25). For an electronic device like the one depicted in Fig. 1(a), the electrostatic potential in the left and right contact is set by the applied bias. The potential in the central region must therefore be obtained from the Poisson equation

$$\nabla^2\delta V_H(\boldsymbol{r}) = -4\pi\delta n(\boldsymbol{r}), \tag{28}$$

under these boundary conditions. In our approach, the device density matrix $\boldsymbol{\sigma}(t)$ is used to compute time-dependent Mulliken charges according to Eq. (22), which are used to set up the difference density $\delta n(\boldsymbol{r})$ via Eq. (20). Taking $\tau_\alpha = \frac{16}{5}U_\alpha$ as above, some exchange and correlation effects are taken into account at this point, since the Hubbard-like parameters $U_\alpha$ stem from a DFT calculation and are considerably smaller than unscreened Hartree-only parameters [36].

The Poisson equation is then discretized on a grid and solved in real space for a sufficiently large box enclosing the device region. Note that an inherent assumption of such an approach is that the potential at the device-lead interface equals the potential in the contact interior. In other words, the device region should include enough layers of the contact material to ensure efficient screening.

Similar to the electron density, $\delta V_H(\boldsymbol{r})$ is projected on the atomic sites through

$$\delta V_\alpha = \frac{1}{\lambda}\int_{\mathrm{box}} d\boldsymbol{r}\delta V_H(\boldsymbol{r})e^{-\tau_\alpha|\boldsymbol{r}-\boldsymbol{R}_\alpha|}, \tag{29}$$

with normalization factor $\lambda = \int_{\mathrm{box}} d\boldsymbol{r}e^{-\tau_\alpha|\boldsymbol{r}-\boldsymbol{R}_\alpha|}$. The required second term in the device Hamiltonian Eq. (26) may now be evaluated as

$$\delta V_{\mu\nu} = \frac{1}{2}(\delta V_\alpha + \delta V_\beta) S_{\mu\nu}, \quad \mu \in \alpha,\ \nu \in \beta. \tag{30}$$

Please note that the overlap matrix $\boldsymbol{S}$ is non-diagonal in the DFTB approach, while the results of Section 2 were derived for an orthogonal basis. The necessary adaptions of the theory are straightforward and discussed in detail in [1, Chapter 8.1.2]. It should also be mentioned, that the approach discussed in this subsection follows the work of Pecchia et al. [37], who earlier implemented the static Landauer formalism for the DFTB method.

#### 3.2.2. Self-energy

From Eq. (8), the retarded self-energy function $\boldsymbol{\Sigma}^r_\alpha$ can be expressed in the energy domain as

$$\boldsymbol{\Sigma}^r_\alpha(E) = \boldsymbol{T}^\dagger_\alpha \boldsymbol{g}^r_\alpha(E) \boldsymbol{T}_\alpha, \tag{31}$$

where $\boldsymbol{g}^r_\alpha$ is the retarded Green's function of the $\alpha$th contact. As in previous work, we assume that the contacts are semi-infinite periodic lattices, which are divided into principle layers (PLs) along the transport direction. The PLs are chosen so wide that only interactions between nearest PLs need to be considered. Then the coupling matrix $\boldsymbol{T}_\alpha$ between contact and device region (which includes at least one PL in the device part) will be restricted to one PL, and only the surface block of $\boldsymbol{g}^r_\alpha$, the *surface* Green's function $\boldsymbol{g}^s_\alpha(E)$, is needed to calculate $\boldsymbol{\Sigma}^r_\alpha$.

The surface Green's function $\boldsymbol{g}^s_\alpha(E)$ can be obtained from the standard renormalization method [38]. Denoting $\boldsymbol{H}_{00}$ as the Hamiltonian of one PL, and $\boldsymbol{H}_{01}$ as the coupling matrix between the nearest PL, $\boldsymbol{g}^s_\alpha$ is given by

$$\boldsymbol{g}^s_\alpha(E) = (E\boldsymbol{I} - \zeta_\infty)^{-1}, \tag{32}$$

where the matrices $\zeta_i$ are calculated from the recurrence relations

$$\zeta_{i+1} = \zeta_i + \boldsymbol{a}_i (E\boldsymbol{I} - \boldsymbol{\eta}_i)^{-1} \boldsymbol{b}_i, \tag{33}$$

$$\boldsymbol{\eta}_{i+1} = \boldsymbol{\eta}_i + \boldsymbol{a}_i (E\boldsymbol{I} - \boldsymbol{\eta}_i)^{-1} \boldsymbol{b}_i + \boldsymbol{b}_i (E\boldsymbol{I} - \boldsymbol{\eta}_i)^{-1} \boldsymbol{a}_i, \tag{34}$$

$$\boldsymbol{a}_{i+1} = \boldsymbol{a}_i (E\boldsymbol{I} - \boldsymbol{\eta}_i)^{-1} \boldsymbol{a}_i, \tag{35}$$

$$\boldsymbol{b}_{i+1} = \boldsymbol{b}_i (E\boldsymbol{I} - \boldsymbol{\eta}_i)^{-1} \boldsymbol{b}_i \tag{36}$$

with the initial matrices $\zeta_0 = \boldsymbol{H}_{\alpha,00}$, $\boldsymbol{\eta}_{\alpha,0} = \boldsymbol{H}_{\alpha,00}$, $\boldsymbol{a}_0 = \boldsymbol{H}_{\alpha,01}$, $\boldsymbol{b}_0 = \boldsymbol{H}^\dagger_{\alpha,01}$. In the simplest approximation, the PL matrices $\boldsymbol{H}_{\alpha,00}$ and $\boldsymbol{H}_{\alpha,01}$ are obtained from a conventional DFTB calculation in which the contact is treated as a finite cluster. Although the semi-infinite nature of the contacts is still accounted for by the renormalization method, computational artefacts have recently been reported for this approach [39]. Instead, we obtain the PL matrices from simulations using periodic boundary conditions with converged Brillouin zone sampling [40].

After construction of the surface Green's function $\boldsymbol{g}^s_\alpha(E)$, it is straightforward to compute the self-energy at the Fermi energy

$$\boldsymbol{\Sigma}^r_\alpha(E_F) = \boldsymbol{H}^\dagger_{\alpha,01} \boldsymbol{g}^s_\alpha(E_F) \boldsymbol{H}_{\alpha,01}, \tag{37}$$

which provides the necessary parameters for the wide-band approximation used to determine the dissipation term $\boldsymbol{Q}_\alpha$.

#### 3.2.3. Initial density matrix

We assume that the device is in thermal equilibrium at $t = 0$ with a common Fermi energy for the full lead-device-lead system. Only for $t > 0$ a bias is applied which drives the central region out of equilibrium and results in a current flow. The initial conditions for the solution of our central Eq. (10) may therefore be obtained from equilibrium Green's function theory. For the reduced density matrix $\boldsymbol{\sigma}(0)$ we have

$$\boldsymbol{\sigma}(0) = \int_{-\infty}^{+\infty} \frac{dE}{2\pi} f(E) \Im\{\boldsymbol{G}^r(E)\}, \tag{38}$$

where $\Im\{\boldsymbol{G}^r\}$ is the imaginary part of retarded Green's function

$$\boldsymbol{G}^r(E) = [E\boldsymbol{I} - \boldsymbol{H}(0) - \boldsymbol{\Sigma}^r(E)]^{-1}. \tag{39}$$

Notice that $\boldsymbol{H}(0)$ is determined by $\boldsymbol{\sigma}(0)$ through Eqs. (26) and (30), thus the above equations need to be solved self-consistently. Compared with the conventional DFTB scheme for closed systems, Eq. (38) replaces the secular Eq. (24) to obtain the density matrix, while Eq. (26) replaces Eq. (25) to construct the Hamiltonian.

After obtaining the initial conditions $\boldsymbol{\sigma}(0)$ and $\boldsymbol{H}(0)$, we use the Runge–Kutta method to propagate the density matrix $\boldsymbol{\sigma}(t)$ with a time step $\Delta t$ of 0.02 fs. Solution of the Poisson equation allows the Hamiltonian $\boldsymbol{H}(t)$ to be updated according to Eq. (26). In this approach, $\boldsymbol{H}(t)$ depends only on the density at time $t$ and not on densities at former times, which corresponds to the adiabatic approximation for exchange and correlation. Finally, the dissipation term $\boldsymbol{Q}_\alpha(t)$ is calculated from Eq. (14) to compute the current and $\boldsymbol{\sigma}(t + \Delta t)$. This completes the discussion on the implementation of the TD-DFTB method for open systems.

## 4. Test calculations

The method described above has been applied to two prototypical molecular junctions: a carbon chain with metallic transport properties and an oxygen anchored benzene molecule with small linear response conductance. In Section 4.1 we will discuss the establishment of a steady state for asymptotically constant bias potential, while Section 4.2 is devoted to a comparison with *first principles* TDDFT results in order to classify the accuracy of our approximate scheme.

### 4.1. Development of steady state

The first system we study here is a carbon chain which bridges two aluminum wires as shown in Fig. 1(b). The chain consists of seven carbon atoms with a distance of 1.32 Å between nearest neighbors. The electrodes are given by Al nanowires of finite cross sections oriented in (001) direction. The two end carbon atoms of the chain are located at the hollow sites of the surfaces, and the distance between the end atom and the first layer of the Al surface is 1.0 Å. Each PL in the electrodes comprises 18 Al atoms. Besides the carbon chain, two adjacent PLs are included in the device region amounting to 43 atoms in total. Similar systems have been studied by several authors with the DFT-NEGF method [41–43]. Thus, it serves as a good test model for our purposes here.

In an initial application of the TD-DFTB scheme, we apply a time dependent bias potential that is exponentially turned on with a time constant $T$ and approaches a constant value $V_0$ asymptotically:

$$V_L = 0, \quad V_R(t) = V^0_R(1 - e^{-t/T}). \tag{40}$$

Fig. 2 depicts the current traces for various time constants $T$. Although the initial transient currents differ considerably, the same final steady state current is reached in all cases. This is a non-trivial result, as earlier model studies indicated the possibility of multiple steady state solutions [44], or even the absence of a steady state [22,45]. The latter investigations by Khosravi and co-workers predict persistent current oscillations if the device region supports a bound state which is uncoupled to the leads.

The existence of such undamped solutions may also be deduced in the present formalism. If we assume that $\boldsymbol{\sigma}(t)$ and $\boldsymbol{H}(t)$ approach constant values at $t_s$ such that

$$\boldsymbol{\sigma}(t_s) \approx \boldsymbol{\sigma}(\infty) \wedge \boldsymbol{H}(t_s) \approx \boldsymbol{H}(\infty), \tag{41}$$

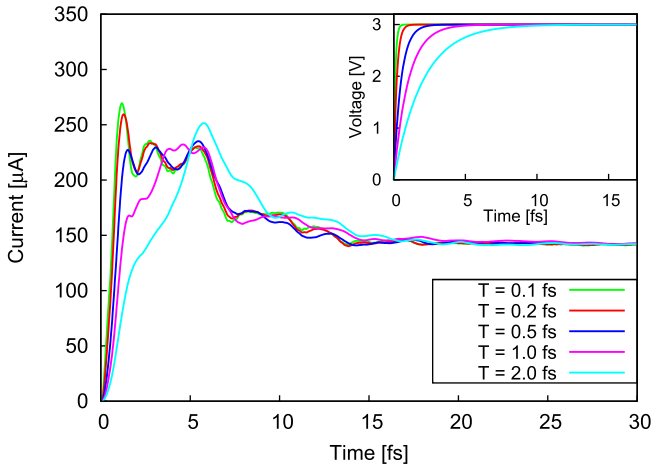


**Fig. 2.** TD-DFTB transient currents through the carbon chain of Fig. 1(b) for an exponential turn on of the bias with different time constants $T$. The inset shows the time dependent bias approaching $V_R^0 = 3$ V.

the last part in the dissipation term $\boldsymbol{Q}_\alpha$ of Eq. (14) may be decomposed into

$$\boldsymbol{K}_\alpha(t) = \boldsymbol{K}_\alpha^\infty + \widetilde{\boldsymbol{K}}_\alpha(t) \tag{42}$$

for $t > t_s$. Here $\boldsymbol{K}_\alpha^\infty$ is given by

$$\boldsymbol{K}_\alpha^\infty = -\frac{2i}{\pi}\int_{-\infty}^{\mu_0} \frac{d\epsilon}{\left(\epsilon - V_\alpha^0\right)\boldsymbol{I} - \boldsymbol{H}(\infty) - \boldsymbol{\Sigma}^r}\boldsymbol{\Lambda}_\alpha + \text{h.c.} \tag{43}$$

and contributes to the steady state current, while the component

$$\widetilde{\boldsymbol{K}}_\alpha(t) = -\frac{2i}{\pi}\int_{-\infty}^{\mu_0} d\epsilon \exp\left[i\left\{\left(\epsilon - V_\alpha^0\right)\boldsymbol{I} - \boldsymbol{H}(\infty) - \boldsymbol{\Sigma}^r\right\}(t-t_s)\right]\boldsymbol{\kappa}_\alpha^\infty(\epsilon) + \text{h.c.}$$

with

$$\boldsymbol{\kappa}_\alpha^\infty(\epsilon) = e^{i\epsilon t_s}\boldsymbol{U}_\alpha(t_s)\left[\frac{1}{\epsilon\boldsymbol{I} - \boldsymbol{H}(0) - \boldsymbol{\Sigma}^r} - \frac{1}{\left(\epsilon - V_\alpha^0\right)\boldsymbol{I} - \boldsymbol{H}(\infty) - \boldsymbol{\Sigma}^r}\right]\boldsymbol{\Lambda}_\alpha, \tag{44}$$

might give rise to permanent oscillations of the current beyond $t_s$. This occurs if at least one of the eigenvalues of the effective device Hamiltonian $\boldsymbol{H} + \boldsymbol{\Sigma}^r$ is purely real, i.e. a bound state exists which is completely uncoupled from the contacts. As an additional trivial prerequisite, al least one transmitting channel must be coupled to the leads, otherwise $\boldsymbol{\Lambda}$ and therefore also the current vanish. In all of our practical simulations so far, we never encountered such a situation of permanent current oscillations.

### 4.2. Comparison with TDDFT

In this section we benchmark the approximate TD-DFTB scheme against results obtained with the LODESTAR code, that implements the reduced density matrix propagation method of Section 2 at the full TDDFT level. Throughout the paper the Perdew–Burke–Ernzerhof exchange–correlation functional is employed for TD-DFTB and the TDDFT calculations are performed in the adiabatic LDA. Two different Gaussian-type basis sets are used in the latter: the STO-3G set is roughly of the same size as the minimal DFTB basis, while the more accurate 6–31G set is a split-valence basis of double-$\zeta$ quality.

We will first discuss the regime of linear response with small bias. Results for the temporal bias profile of Eq. (40) with $T = 1$ fs and $V_R^0 = 0.1$ mV are given in Fig. 3. Currents can be evaluated at either the left or right lead-device interface. In the initial phase these current may in principle differ in magnitude, indicating a transient charging and decharging of the device. In the steady state both need to be equal, which provides a stringent test for the numerical accuracy of the implementation.

Comparison of the current traces shows that a steady state is reached in roughly 5 fs, although especially in the TDDFT/STO-3G and TD-DFTB methods small amplitude oscillations are observed which fully die out only after several tenths of fs. The fact that the current does not follow the bias instantaneously was related to a kinetic inductance in Ref. [46], which originates from the inertia or effective mass of the carriers in the leads. Focussing now on the long time limit and taking the 6–31G results as reference, the steady state currents of TD-DFTB and TDDFT/STO-3G show a deviation of roughly 30 %. The conductance of the latter is with $G = 1.1$ $G_0$ ($G_0 = 77.48$ μS) in good agreement with the single-$\zeta$ results of Ke et al. [43].

One drawback of time-dependent transport simulations are the limited options to analyze the outcome. In contrast, static

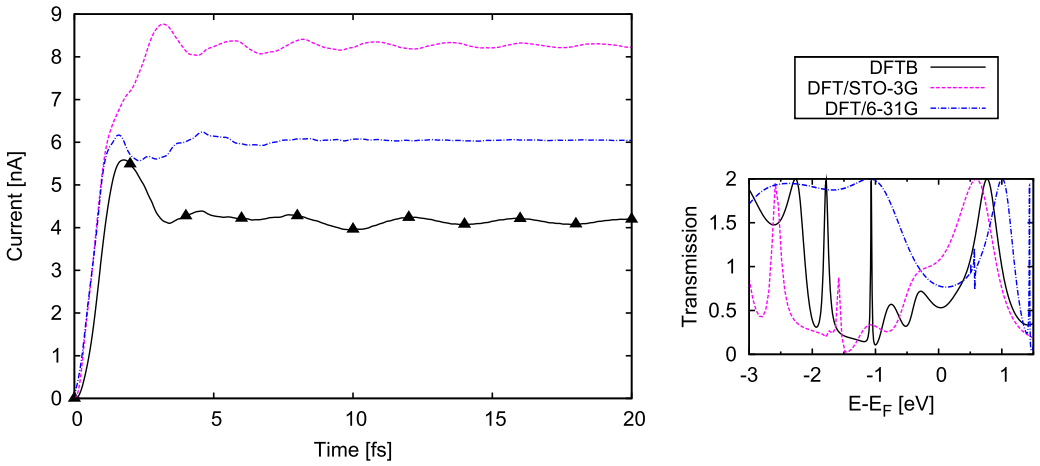


**Fig. 3.** Left figure: Time dependent currents for the carbon chain device of Fig. 1(b) as given by TD-DFTB and TDDFT using the LDA exchange–correlation functional with the two basis sets STO-3G and 6–31G. Simulation parameters: $V_L = 0$ V, $V_R^0 = 0.1$ mV, T = 1 fs. The solid line for the TD-DFTB method is the current at the left lead-device interface, while the filled triangles give the current at the right lead-device interface. Right figure: Transmission functions T(E) at $V = 0$ V obtained from the static DFT-NEGF approach at the respective level of theory.

DFT-NEGF simulations are usually discussed in the framework of Landauer transport theory which features a bias and energy dependent transmission function T(E, V) as key object [1]. The transmission provides detailed information on the molecular resonances, as well as on the device-lead coupling and the transparency of individual transport channels. *A priori*, it is not obvious that TDDFT simulations follow the Landauer picture and recent investigations show that this is indeed not the case [15–17]. Using local or semi-local exchange–correlation functionals, however, steady state TDDFT and static DFT-NEGF currents agree with high precision [18]. For the present system we find for example a DFTB-NEGF current of 4.14 nA compared to a TD-DFTB value of 4.19 nA. In order to facilitate a deeper analysis, Fig. 3 also contains the transmission functions obtained at the different levels of theory from static DFT(B)-NEGF simulations in the WBA. In the linear response regime, the current is governed by the transmission T ($E_F$) at the Fermi energy, which shows the same order (DFT/STO-3G > DFT/6–31G > DFTB) as found for the steady state current. The high transmission of the STO-3G mainly stems from the tail of a transmission channel at 0.5 eV above $E_F$, which is found at higher energies for the other two methods. To the 6–31G transmission at $E_F$ contributes also a broad feature centered around −1.0 eV, which splits into narrower peaks at the DFTB level. This fact indicates a smaller imaginary part of the self-energy for this channel, which might also explain the slower decay of oscillations in the transient TD-DFTB current (Fig. 3 left).

Turning now to current traces at a higher bias value of $V = 1$ V in Fig. 4, we find the two TDDFT results to be close, although this is somewhat coincidental. At finite bias, the current in the Landauer picture is obtained by integrating the transmission over the bias window from 0 V to 1 V as indicated in the figure. For the STO-3G basis the resonance above $E_F$ strongly contributes, whereas only a fraction of this channel resides in the bias window for DFTB and DFT in the more accurate 6–31G basis. DFTB resonances that are located in equilibrium at −0.25 V and −0.75 V with respect to $E_F$ shift into the bias window, but have a small transmission leading to the lower value of the current observed.

The sizable variation of the transmission characteristics among the different methods is also seen for the next device we studied. Fig. 1(c) shows the structure of 1, 4-benzenediol inbetween Al wires of the same kind as in the previous simulations. The DFTB optimized molecule was placed symmetrically into the junction so that the terminating oxygen atoms are positioned on the hollow sites of the Al surfaces at a distance of 1.22 Å. This geometry is also used in the following TDDFT calculations.

Focusing first on the left part of Fig. 5, one observes a strong initial overshoot of the current in all methods, before it reaches a constant value after roughly 5 fs. Again, the DFTB current shows longer

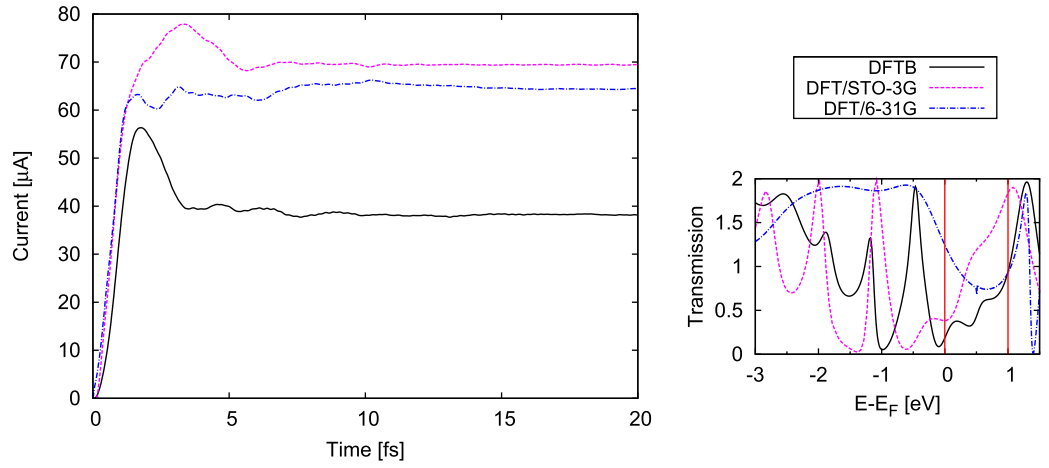


**Fig. 4.** Left figure: Time dependent currents for the carbon chain device. Simulation parameters: $V_L = 0$ V, $V_R^0 = 1.0$ V, T = 1 fs. Right figure: Transmission functions T(E) at $V = 1$ V. The vertical lines indicate the bias window.

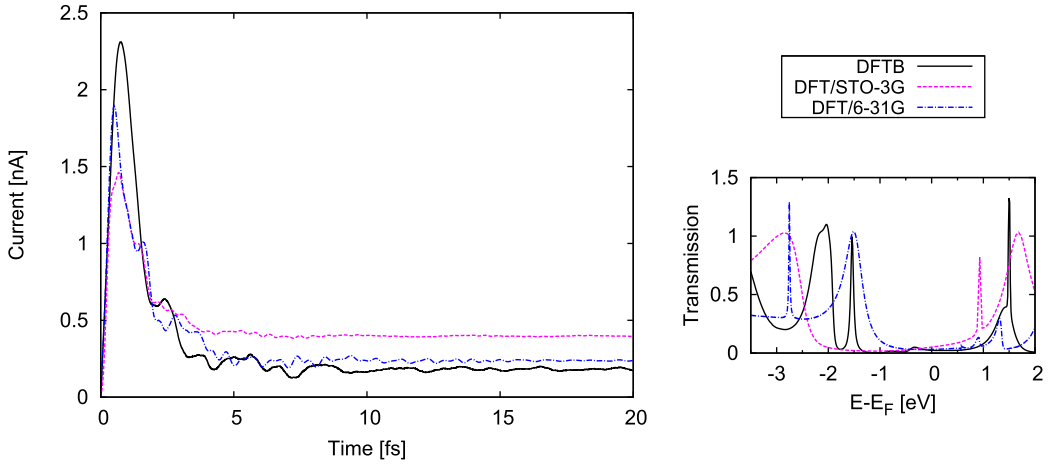


**Fig. 5.** Left figure: Time dependent currents through 1, 4-benzenediol (see Fig. 1(c)). Simulation parameters: $V_L = 0$ V, $V_R^0 = 0.1$ mV, T = 1 fs. Right figure: Transmission functions T(E) at $V = 0$ V.

lasting oscillations than TDDFT/6–31G, but the limiting values agree. Also in the transmission the DFTB results are closer to TDDFT in the larger basis. T(E) features a transmission gap of roughly 2.5–3 eV which is smaller than the corresponding gap for the isolated molecule ($C_6O_2H_6$), for which we find a value of roughly 3.8 eV in all methods. The highest occupied molecular orbital (HOMO) is fully transparent at the DFTB and DFTB/6–31G level and located at −1.5 eV in Fig. 5, with a considerably reduced width in the former method. Inspection of the local density of states (LDOS, not shown here) reveals that also the DFT/STO-3G scheme has a state at −1.9 eV, which carries however no current and does not appear in the transmission. The precise location of the lowest unoccupied molecular orbital (LUMO) is more difficult to access. The LDOS exhibits peaks at approximately 1.5 eV (DFTB), 0.9 eV and 2.0 eV (DFT/STO-3G) and 0.5 eV, 0.9 eV and 1.5 eV (DFT/6–31G), respectively. Judging from the LDOS alone it is difficult to discriminate between molecular states and metal induced gap states that appear due to the presence of the additional Al layers in the extended molecule. The latter are usually localized and do not significantly contribute to the transmission. Taking this into account, we therefore tentatively assign the LUMO state to the resonance at ≈1.5 eV for DFTB and DFT/6–31G as well as ≈2.0 eV for DFT/STO-3G. These observations fit into the general trend observed for gas phase molecules: The DFTB method overestimates HOMO–LUMO gaps in comparison with DFT calculations with converged basis sets, but to a much lesser extent than DFT simulations with a basis of single-$\zeta$ quality [28]. The HOMO–LUMO gap has a strong impact on the transport characteristics of a device[2] and it is known that DFT simulations overestimate conductances. This is due to the fact that the DFT HOMO–LUMO gap is significantly smaller than the true quasiparticle gap, given by the difference of ionization potential and electron affinity. As recently shown by Strange et al. [47], calculations at the GW level of theory are able to overcome this deficiency and provide accurate quasiparticle gaps leading to good agreement between experiment and theory. In this regard, one would expect that the currents obtained from DFTB are closer to experimental values. This is certainly another case of achieving the right result for the wrong reason, but this point could be of interest for investigations targeting pragmatic solutions.

Returning to Fig. 5, it is obvious that $T(E_F)$ and therefore also the current is very sensitive to the precise peak position and broadening of the molecular states. In fact, it is not uncommon that transport simulations using slightly different levels of theory or even different implementations of the same level of theory differ by one order of magnitude in the predicted currents [2]. In this respect, the TD-DFTB scheme falls well into these general error bars.

At the end of this section, we shortly report the required CPU time for the simulations presented. On a single core of an `Intel Xeon X5560@2.80 GHz` multi-core processor, 100 time steps for the carbon chain device took roughly 120 CPU minutes (TDDFT/6–31G), 43 min (TDDFT/STO-3G) and 8 min (TD-DFTB), respectively. For the 1, 4-benzenediol device, the simulations took 139 min (TDDFT/6-31G), 48 min (TDDFT/STO-3G) and 7 min (TD-DFTB), respectively.

## 5. Summary and outlook

In this article, we presented theory, implementation and validation of an approximate TDDFT method for open systems out of equilibrium. The temporal profile of the TD-DFTB current traces was found to be qualitatively similar to *first principles* simulations. A rapid switch leads to an overshoot of the current which settles into a steady state after only a few fs. As in earlier TDDFT simulations [18], a steady state is always reached and does not depend on the history of the applied bias. Notwithstanding, we showed that permanent current oscillations are valid solutions of our employed equations of motion. The absolute value of the steady state currents was then discussed in the language and framework of the conventional static DFT-NEGF formalism. We found that TD-DFTB and TDDFT can differ significantly from each other, but this difference is not larger than the one between full TDDFT calculations using different basis sets. With respect to computational efficiency, the TD-DFTB approach is roughly one order of magnitude faster than a *first principles* implementation in the same formalism.

A limitation of the presented approach is related to applications which require a large bias voltage of several V. In this case also molecular resonances far away from the frontier orbitals are moving into the bias window which, especially for the unoccupied states, are insufficiently described at a minimal basis set level. As mentioned earlier, it is entirely possible to include higher angular momentum states in the DFTB basis, although the two-center approximation for the Hamiltonian matrix elements becomes less accurate in this case. A larger basis does therefore not necessarily lead to a better result.

The main advantage of the TD-DFTB scheme is its computational efficiency. This allows for important extensions which are not easily realizable in a *first principles* framework. To this class belongs for example the implementation of the hierarchical equation of motion approach [24], which goes beyond the wide band approximation for the leads. Conceivable is also the consideration of quasiparticle corrections to the transport gap. For the static case, such GW calculations have already been performed within the DFTB framework [36,48]. Having applications to molecular photoswitches in mind, another important extension would be the realization of molecular dynamics simulations under current flow involving time-dependent external fields. Efforts in this direction are currently under way.

[2] More precisely, the equilibrium conductance is most strongly influenced by the level closest to $E_F$. Since $E_F$ is often located in the middle of the HOMO–LUMO gap, the size of the latter is also determining the transport gap.

## Acknowledgement

The authors thank the German Science Foundation (SPP 1243 *Quantum transport at the molecular scale*) for financial support.

## References

[1] J.C. Cuevas, E. Scheer, Molecular Electronics: An Introduction to Theory and Experiment, World Scientific, 2010.
[2] S.M. Lindsay, M.A. Ratner, Adv. Mater. 19 (1) (2007) 23.
[3] L.P. Kadanoff, G. Baym, Quantum Statistical Mechanics: Green's Function Methods in Equilibrium and Nonequilibrium Problems, Addison-Wesley, 1989.
[4] R. Landauer, IBM J. Res. Dev. 1 (1957) 233.
[5] M. Büttiker, Phys. Rev. Lett. 57 (14) (1986) 1761.
[6] J.K. Tomfohr, O.F. Sankey, Phys. Stat. Sol. B 226 (1) (2001) 115.
[7] R. Baer, T. Seideman, S. Ilani, D. Neuhauser, J. Chem. Phys. 120 (2004) 3387.
[8] K. Burke, R. Car, R. Gebauer, Phys. Rev. Lett. 94 (14) (2005) 146803.
[9] N. Bushong, N. Sai, M. Di Ventra, Nano Lett. 5 (2005) 2569.
[10] S. Kurth, G. Stefanucci, C.O. Almbladh, A. Rubio, E.K.U. Gross, Phys. Rev. B 72 (3) (2005) 35308.
[11] C. Cheng, J. Evans, T. Van Voorhis, Phys. Rev. B 74 (2006) 155112.
[12] X. Zheng, F. Wang, C.Y. Yam, Y. Mo, G.H. Chen, Phys. Rev. B 75 (19) (2007) 195127.
[13] J. Evans, O. Vydrov, T. Van Voorhis, J. Chem. Phys. 131 (2009) 034106.
[14] G. Stefanucci, C.O. Almbladh, Phys. Rev. B 69 (19) (2004) 195318.
[15] F. Evers, F. Weigend, M. Koentopp, Phys. Rev. B 69 (23) (2004) 235411.
[16] N. Sai, M. Zwolak, G. Vignale, M. Di Ventra, Phys. Rev. Lett. 94 (18) (2005) 186810.
[17] G. Vignale, M. Di Ventra, Phys. Rev. B 79 (1) (2009) 14201.
[18] C.Y. Yam, X. Zheng, G.H. Chen, Y. Wang, T. Frauenheim, T.A. Niehaus, Time-dependent versus static quantum transport simulations beyond linear response. Available from: <arXiv:1101.0722v1>.
[19] M. Koentopp, C. Chang, K. Burke, R. Car, J. Phys. Condens. Matter 20 (2008) 083203.

[20] G. Stefanucci, S. Kurth, E. Gross, A. Rubio, Molecular and Nano Electronics: Analysis, Design and Simulation, Elsevier Science Ltd, 2006. p. 247 (Chapter 10).
[21] G. Stefanucci, S. Kurth, A. Rubio, E. Gross, Phys. Rev. B 77 (2008) 75339.
[22] E. Khosravi, G. Stefanucci, S. Kurth, E. Gross, Phys. Chem. Chem. Phys. 11 (2009) 4535.
[23] C.Y. Yam, Y. Mo, F. Wang, X. Li, G.H. Chen, X. Zheng, Y. Matsuda, J. Tahir-Kheli, A.G. William III, Nanotech. 19 (2008) 495203.
[24] X. Zheng, G.H. Chen, Y. Mo, S.K. Koo, H. Tian, C.Y. Yam, Y.J. Yan, J. Chem. Phys. 133 (2010) 114101.
[25] G. Seifert, H. Eschrig, W. Bieger, Z. Phys. Chem. (Leipzig) 267 (1986) 529.
[26] D. Porezag, T. Frauenheim, T. Köhler, G. Seifert, R. Kaschner, Phys. Rev. B 51 (19) (1995) 12947.
[27] M. Elstner, D. Porezag, G. Jungnickel, J. Elsner, M. Haugk, T. Frauenheim, S. Suhai, G. Seifert, Phys. Rev. B 58 (11) (1998) 7260.
[28] T.A. Niehaus, S. Suhai, F. Della Sala, P. Lugli, M. Elstner, G. Seifert, T. Frauenheim, Phys. Rev. B 63 (8) (2001) 085108.
[29] T.A. Niehaus, D. Heringer, B. Torralva, T. Frauenheim, Eur. Phys. J. D 35 (3) (2005) 467.
[30] T.A. Niehaus, J. Mol. Struct. Theochem. 914 (2009) 38.
[31] H. Haug, A.P. Jauho, Quantum Kinetics in Transport and Optics of Semiconductors, Springer Verlag, 2008.
[32] T. Frauenheim, G. Seifert, M. Elstner, T. Niehaus, C. Köhler, M. Amkreutz, M. Sternberg, Z. Hajnal, A. Di Carlo, S. Suhai, J. Phys. Condens. Matter 14 (11) (2002) 3015.
[33] G. Seifert, J. Phys. Chem. A 111 (26) (2007) 5609, doi:10.1021/jp069056r. Available from: <http://pubs.acs.org/doi/pdf/10.1021/jp069056r>.
[34] N. Otte, M. Scholten, W. Thiel, J. Phys. Chem. A 111 (26) (2007) 5751.
[35] J.C. Slater, G.F. Koster, Phys. Rev. 94 (6) (1954) 1498.
[36] T.A. Niehaus, M. Rohlfing, F. Della Sala, A. Di Carlo, T. Frauenheim, Phys. Rev. A 71 (2) (2005) 022508.
[37] A. Pecchia, G. Penazzi, L. Salvucci, A. di Carlo, New J. Phys. 10 (2008) 065022.
[38] M.P. López Sancho, J.M. López Sancho, J.M.L. Sancho, J. Rubio, J. Phys. F: Met. Phys. 15 (1985) 851.
[39] A. Beste, V. Meunier, R.J. Harrison, J. Chem. Phys. 128 (2008) 154713.
[40] B. Aradi, B. Hourahine, T. Frauenheim, J. Phys. Chem. A 111 (26) (2007) 5678.
[41] B. Larade, J. Taylor, H. Mehrez, H. Guo, Phys. Rev. B 64 (7) (2001) 75420.
[42] M. Brandbyge, J.L. Mozos, P. Ordejon, J. Taylor, K. Stokbro, Phys. Rev. B 65 (16) (2002) 165401.
[43] S.H. Ke, H.U. Baranger, W. Yang, Phys. Rev. B 70 (8) (2004) 85410.
[44] C.G. Sánchez, M. Stamenova, S. Sanvito, D.R. Bowler, A.P. Horsfield, T.N. Todorov, J. Chem. Phys. 124 (2006) 214708.
[45] E. Khosravi, S. Kurth, G. Stefanucci, E.K.U. Gross, Appl. Phys. A 93 (2) (2008) 355.
[46] S.H. Ke, R. Liu, W. Yang, H.U. Baranger, J. Chem. Phys. 132 (2010) 234105.
[47] M. Strange, C. Rostgaard, H. Häkkinen, K.S. Thygesen, Phys. Rev. B 83 (11) (2011) 115108, doi:10.1103/PhysRevB.83.115108.
[48] A. Gagliardi, A. Pecchia, T.A. Niehaus, T. Frauenheim, A. Di Carlo, Quasiparticle correction for electronic transport in molecular wires, J. Comput. Electron. 6 (2007) 345.